Optics Letters

Tunable dissipative soliton Tm-doped fiber laser operating from 1700 nm to 1900 nm

Xinyang Liu,[1,*] Jayanta K. Sahu,[2] and Regina Gumenyuk[1,3]

[1]Laboratory of Photonics, Tampere University, Korkeakoulunkatu 3, Tampere 33720, Finland
[2]Optoelectronics Research Centre, University of Southampton, Highfield, Southampton, SO17 1BJ, UK
[3]Tampere Institute for Advanced Study, Tampere University, Kalevantie 4, Tampere 33100, Finland
*Corresponding author: xinyang.liu@tuni.fi

Received 21 October 2022; revised 23 November 2022; accepted 29 November 2022; posted 29 November 2022; published 20 January 2023

In this Letter, we demonstrate an ultrabroadband (1700–1900 nm) tunable Tm-doped fiber laser (TDFL) generating dissipative solitons in the net-normal dispersion regime. The laser delivers pulses with spectral widths ranging from 10 nm to 23 nm and pulse durations from 8.7 ps to 18.3 ps. Stretched-free pulse amplification at the gain edge (1708 nm) and gain peak (1807 nm) is implemented to demonstrate the range of further power scalability of the laser signal. The maximum achieved power in a one-stage Tm-doped amplifier is 140 mW with a compressed pulse duration of 478 fs. Considering the diverse utility of this wavelength band, this laser is highly desirable for applications such as optical sensing, biological imaging, and industrial machining.

https://doi.org/10.1364/OL.478838

Benefiting from strong Stark splitting of $^3F_4$ and $^3H_6$ energy levels of the Tm^{3+} ion, a Tm-doped silica fiber has the broadest fluorescence spectrum among rare-earth-doped fibers, which exceeds 500 nm [1], ranging from 1.6 μm to 2.2 μm. This wavelength band is of great research interest since it fulfils the need for many practical applications. In the age of information explosion, there is a strong need to extend the conventional communication band (~1.5 μm) to a longer wavelength with the emergence of low-loss hollow-core photonic fiber [2]. Taking advantage of the first overtone band (~1725 nm) of the C–H bond, the laser source in this wavelength region is ideal for methane sensing and polymer welding [3], and in particular this wavelength band appears retina-safe. In medical surgery, due to water absorption local minima in this wave band mean preferential targeting of lipid-rich tissue can be achieved [4]. Three-photon microscopy (3PM) at this wavelength band, compared with commonly used first (650–950 nm) and second (1100–1350 nm) biological windows, has the merits of reduced scattering (thus deeper penetration depth into tissue), improved signal-to-noise ratio (SNR), and diminished phototoxicity [5]. A tunable laser source is of particular interest as it can be used to select the optimal wavelength and increases the number of accessible fluorophores in 3PM.

Considerable research effort has been put into the long-wavelength-band (>1800 nm) operation of Tm-doped fiber lasers (TDFLs), including ultrafast laser pulse generation [6,7], wavelength-tunable operation [8], and high repetition rate operation [9]. For the short-wavelength-band (<1800 nm), despite its tremendous potential for the above-mentioned applications, comprehensive investigation was not carried out until recent years due to the significantly lower gain coefficient and, as a consequence, strong dependency on low-loss components. Initial research effort focused on the continuous-wave (CW) regime of TDFLs and Tm-doped fiber amplifiers (TDFAs), including single-frequency and wavelength-tunable operation [10–13]. In these works, to suppress high gain at longer wavelengths, different approaches have been employed, such as incorporating wavelength-selective components including fiber Bragg gratings (FBGs), tunable filters, and photonic crystal fibers (PCFs), and deploying absorption characteristics of Tb^{3+} and Ho^{3+} ions. With successful suppression of the longer-wavelength gain, ultrafast operation of TDFLs at the short-wavelength-band was investigated. In a conventional soliton regime, the wideband tunable mode-locking operation was realized by introducing fiber-bending loss, PCF, an acousto-optic tunable filter (AOTF), and a combination of gratings and slits [14–17]. However, the conventional soliton regime has the intrinsic drawback that the output pulse energy is limited by the soliton area theorem and the soliton pulses are not suitable for further amplification due to the pronounced background of dispersive waves. In 2021, a dissipative soliton operation was demonstrated, and further chirped pulse amplification was implemented [18,19]. However, the seed laser can only operate at one fixed wavelength. In real-life applications, a laser source with wavelength tunability is essential for choosing the optimal wavelength. Thus, a wavelength-tunable dissipative soliton laser source with pure signal power scalability at this wavelength band is highly desired.

In this Letter, we present an ultrabroadband tunable TDFL followed by a stretched-free fiber-based amplifier. The laser operates in a dissipative soliton regime through intracavity dispersion management and is mode-locked by hybrid mode-locking techniques of nonlinear polarization rotation (NPR) and frequency shifting feedback (FSF). The intracavity laser tuning in the wavelength range of 1700–1900 nm is realized by an AOTF. The laser emits directly ultrafast pulses within the whole tuning range with spectral widths from 10 nm to 23 nm and pulse durations from

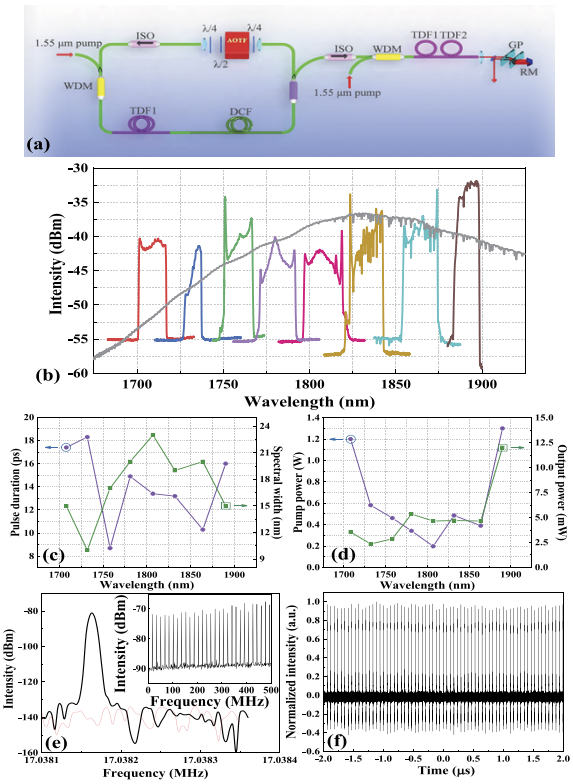

Fig. 1. (a) Experimental setup. WDM: wavelength division multiplexer; TDF: Tm-doped fiber; DCF: dispersion compensation fiber; λ/4: quarter wave plate; λ/2: half wave plate; AOTF: acousto-optic tunable filter; ISO: isolator; GP: grating pair; RM: roof mirror. (b) Wavelength tunability of the Tm-doped dissipative soliton laser with gray line showing amplified spontaneous emission (ASE); (c) spectral widths and pulse durations, (d) pump powers and output powers of seed laser at different wavelengths in the mode-locking operation regime; (e) RF spectra with 10 Hz resolution bandwidth in a 500 Hz span and (the inset) with 10 kHz resolution bandwidth in a 500 MHz span; the red line is the baseline; (f) A typical pulse train.

8.7 ps to 18.3 ps. The further possible power scalability range is demonstrated by signal amplification in a single-stage TDFA at the gain edge (1708 nm) and gain peak (1807 nm). Maximum output powers after the amplifier are 31.5 mW (gain edge) and 141 mW (gain peak) with corresponding compressed pulse durations of 523 fs and 478 fs, respectively.

The experimental setup is shown in Fig. 1(a). It comprises a seed laser, one amplifier stage, and a pulse compressor. Two self-made master oscillator power amplifiers (MOPAs) at 1.55 μm with maximum output powers of 2.2 W and 2.7 W serve as pump sources for a seed laser and an amplifier, respectively. Wideband wavelength division multiplexers (WDMs) with a signal transmission band of 1700–2100 nm combine a pump and a signal channel. An intracavity polarization-independent isolator (ISO) ensures unidirectional operation. Two quarter waveplates (QWPs) and one half wave plate (HWP) are placed near the AOTF to control polarization evolution in the cavity. The AOTF (AOTF8, AA Opto-Electronic) provides a spectral filtering effect with a Gaussian-like transmission profile and bandwidths from 11 nm at a wavelength of 1700 nm, to 13.7 nm at a wavelength of 1900 nm [20]. After the AOTF, first-order linearly polarized diffracted light is coupled back into the cavity; therefore, the AOTF also works as a polarizer, which in cooperation with the QWPs and HWP enables mode-locking based on NPR. Apart from that, the AOTF applies a frequency shift to incident light which adds a supplementary mechanism for stabilizing mode-locked laser pulses [21]. The amount of frequency shift depends on the frequency applied by the AOTF driver. For the AOTF in this experiment, the driving frequency varies from 35.9 MHz to 40 MHz, corresponding to a center wavelength of diffracted light from 1892 nm to 1708 nm. 80% power is extracted from the cavity through an output coupler while a 75-cm Tm-doped fiber (OFS, TmDF200) provides gain and a 7.1-m UHNA4 fiber is used for dispersion compensation. The other fiber in the cavity is SMF28. The whole cavity contains 11.5 m fiber and a 43 cm free space section generating pulses with a fundamental repetition rate at ~17 MHz. The total net cavity dispersion is varied along the tuning range and estimated as 0.42 ps^2 at 1734 nm [22]. We estimate the overall cavity loss is ~88% without taking the gain fiber absorption into account, where 40% losses are introduced by the free space part. A single amplification stage is constructed by two Tm-doped fibers with a total length of ~75 cm to demonstrate the possibility for power scalability of the tunable laser in a stretched-free configuration. The amplified signal power is limited by the availability of the pump source.

Figure 1(b) illustrates spectra obtained from the tunable dissipative soliton TDFL with the wideband spontaneous emission presented as a gray line. The spectral widths vary from 10 nm to 23 nm, as shown in Fig. 1(b). Several parameters affect spectral widths at different wavelengths. The transmission bandwidth of the AOTF changes from 11 nm to 13.7 nm within the tunable wavelength range. Rotation angles of the QWPs and HWP need to be set at different values to let the laser operate at the mode-locking regime at different wavelengths. This changes the saturation intensity and modulation depth of the NPR-induced saturable absorption effect [23], leading to variation in laser performance. Varying net cavity dispersions within the broad tuning range can also impact the spectral widths, as well as the spectral profile [24]. Additionally, the spectral profiles are also shaped by the gain profile.

At wavelengths longer than 1825 nm, water absorption lines are very evidently presented on the spectra, inevitably deteriorating pulse quality. Laboratory relative humidity is around 25% when the experiment is implemented. A fiber-coupled AOTF could reduce the length of the free space section and controlled lab humidity could effectively alleviate this issue. The pulse duration is measured by second harmonic generation (SHG)-based autocorrelation. Pulse durations vary from 8.7 ps to 18.3 ps within the tuning range [Fig. 1(c)]. Output powers fall into the range of 2 mW to 5 mW [Fig. 1(d)], except for the longest wavelength operation, which is 12 mW. This is caused by the increased pump power for mode-locking operation at this wavelength [Fig. 1(d)] because the AOTF approaches the longest edge of its working wavelength, and the diffraction efficiency is decreased. At the shortest wavelength (~1708 nm), the required pump power for mode-locking operation is also high. This results from the much lower gain provided by Tm-doped fiber at the gain edge. The lowest required pump power for dissipative soliton operation is at 1807 nm, which is near the gain peak of the active fiber. A typical RF spectrum with a resolution bandwidth of 10 Hz when the laser operates at 1807 nm is shown in Fig. 1(e). The fundamental frequency peaks at 17.038 MHz and

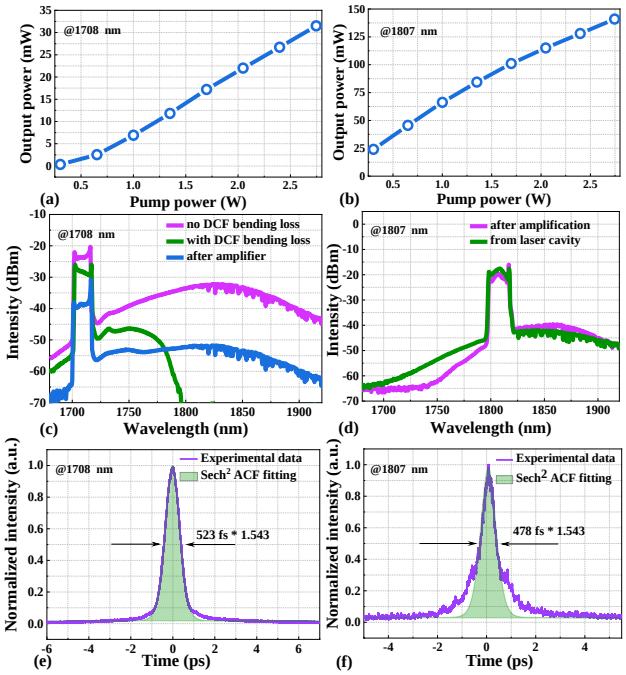

Fig. 2. Amplification power performances, spectra, and autocorrelation traces of compressed pulses, respectively, at (a), (c), and (e) the gain edge of 1710 nm, and (b), (d), and (f) the gain peak of 1807 nm.

has an SNR of 50 dB. The inset of Fig. 1(e) illustrates the RF spectrum in a span of 500 MHz with 10 kHz resolution bandwidth. Together with the pulse train shown in Fig. 1(f), stable single-pulse operation can be confirmed. Similar laser performance has been observed at other wavelengths within the tuning range.

Stretched-free amplification is implemented at the gain edge (1708 nm) and gain peak (1807 nm), respectively, to demonstrate the power scalability of the tunable laser and achievable power range (Fig. 2). The amplifier stage contains ~60 cm TmDF200 fiber (TDF1) with a mode field diameter of 5 μm at 1700 nm and ~15 cm Tm-doped alumina-silicate fiber (TDF2) fabricated using modified chemical vapor deposition (MCVD) and solution-doping techniques at Southampton University with a core diameter of 10 μm and NA ~0.13. Using the cut-back method, the peak absorption coefficient of TDF2 was measured to be ~122 dB/m at 1640 nm. As demonstrated by Elahi *et al.* in Ref. [25], a hybrid amplifier with one piece of low-doped gain fiber followed by high-doped fiber has the overall advantage of low heat generation and low nonlinearity accumulation compared to a single-gain fiber with low or high doping concentration. We have implemented a similar strategy and used the second fiber (TDF2) not only with higher absorption but also with a larger core diameter. TDF2 enables boosting of the output power, utilizing a residual pump while suppressing parasitic lasing at the gain peak. At the gain edge (1708 nm), the maximum output power of 31.5 mW is obtained at the pump power of 2.7 W, corresponding to a gain coefficient of 19.3 dB [Fig. 2(a)] and pulse energy of 1.85 nJ. The low efficiency is caused by the significantly lower gain at this wavelength combined with pump power transfer to the unwanted ASE. The output power grows linearly with pump power with no saturation indication; thus, further power enhancement can be expected with a stronger pump source. To suppress further high gain at longer wavelength, a 1 m dispersion compensation fiber (CYCLE, SM-DCF) is inserted between the ISO and WDM before the amplification stage. By tailoring the fiber bend radius, it is possible to introduce the wavelength-resolved induced loss. The SM-DCF is a single-mode step-index fiber with a core diameter of 5 μm and NA < 0.34 and is prone to be sensitive to bending loss due to its small V number [26]. These losses are wavelength-dependent with the fixed bending radius due to a change of the propagation constant, where longer wavelengths exhibit higher loss [27]. However, incremental change of the bending radius does not result in stepwise change of loss dependency and demonstrates oscillatory features as it is attributed to the coherent coupling between the core propagating field and the field coupling to the cladding and reflected from the cladding–coating interface [27]. It means that in the experiment, the fiber first needs to be coiled to introduce a general wavelength-dependent loss, and then a fine bending is essential to tailor the loss curve to suppress unwanted ASE while preserving the laser signal with minimum loss. In the current experiment, the bending radius of SM-DCF is 9.8 cm. It is worth mentioning that pulses coming from the cavity are strongly chirped, so 1 m of DCF fiber is not enough to stretch pulses and is used as a wavelength-dependent loss-induced element. As a result, the gain at a longer wavelength is effectively suppressed, as shown in Fig. 2(c). After amplification, the spectrum shows no nonlinearity-caused distortion and has an SNR (signal to ASE) of more than 10 dB. Using a pair of gratings with 711 lines/mm groove density, the pulse duration is compressed to 523 fs [see Fig. 2(e)], achieving a pulse duration compression rate of ~34. A little pedestal of the autocorrelation trace also confirms negligible nonlinearity accumulation during amplification. The 1 m SM-DCF is removed when doing amplification at the gain peak (1807 nm). The maximum output power from the amplifier is 141 mW under a pump power of 2.7 W [Fig. 2(b)], corresponding to a pulse energy of 8.2 nJ. No nonlinearity-caused distortion is observed from the spectrum [Fig. 2(d)]. The compressed pulse has a duration of 478 fs, the pulse duration compression rate is ~28. However, the autocorrelation trace of the compressed pulse shows a relatively strong pedestal compared with the one for the gain edge. This results from the higher output power level, making the pulse accumulate more nonlinear chirp [Fig. 2(f)]. For further pulse shape improvement, a stretcher is needed.

To investigate pulse evolution in the cavity and illustrate functionality of different intracavity components, the laser cavity is simulated by numerically solving the generalized Schrödinger equation through the split-step Fourier method using the second-order Runge–Kutta Algorithm [28]. In the simulation, β_2 is set to –0.066 ps^2/m for the SMF28 fiber and Tm-doped fiber and 0.085 ps^2/m for the UHNA4 fiber, resulting in a net dispersion of 0.3 ps^2; γ is set to 0.0023 W^{-1}m^{-1}. An artificial saturable absorber (SA) with 90% modulation depth and 10% saturated loss is placed at the position of the AOTF, simulating the action of NPR. According to the previous study [21], frequency shifting affects mainly the stabilization of pulses in the cavity rather than igniting mode-locking. The spectral filter has a Gaussian profile with an FWHM of 12 nm. After the spectral filter, 30% power loss is added to model the coupling loss. Using white noise as the input, the algorithm can converge to a self-consistent pulse within 100 round trips. The simulation is done at 1800 nm, near the gain peak. Figure 3 depicts

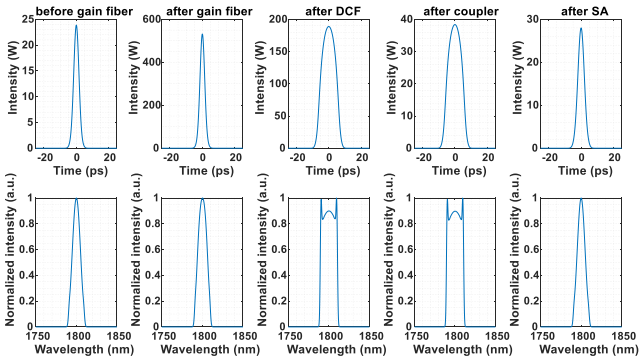

Fig. 3. Simulation results illustrating intracavity pulse and spectrum profiles at different components within one round trip.

intracavity pulse and spectrum profiles at different components, clearly demonstrating their functionalities in pulse propagation. Gain fiber amplifies pulse peak power 22 times while pulse duration stays nearly the same (3.9 ps). The spectrum broadens only slightly (from 11 nm to 13 nm) after the gain fiber. Since only 10 cm of SMF28 fiber is placed between the gain fiber and DCF, its influence on pulse and spectrum is negligible and not illustrated here. After the DCF, the temporal pulse is stretched to 11 ps. A spectrum develops a so-called cat-ear structure with a spectrum width of 21 nm and sharp edges that are the typical feature of dissipative soliton, a result of the dual action of normal dispersion and nonlinearity in the DCF. At the position of the coupler, the pulse duration is slightly compressed to 10.6 ps due to propagation in the SMF 28 fiber with anomalous dispersion, and the spectral width remains at 21 nm, which matches very well with the experimental result. After the SA and spectral filter, the spectrum width is reset to 12 nm, and the temporal pulse is also shortened to 4.6 ps due to its positive chirp.

In this Letter, an ultrabroadband tunable ultrafast TDFL operating between 1700 nm and 1900 nm was demonstrated. The dissipative soliton operation within the whole tunable range was realized by intracavity dispersion management. To achieve state-of-the-art operation with robust laser performance, we have carefully tailored the laser design with an emphasis on the optimum balance of gain and loss combined with an efficiently and widely tunable filter. Due to lasing competition between longer wavelengths with high gain and short wavelengths with low gain, the tunable filter should provide strong wavelength discrimination over a broad wavelength range, which has been possible to realize by the AOTF deflecting only designed wavelengths back into the cavity. With a single-stage amplifier, the stretched-free amplification at the gain edge (1708 nm) and gain peak (1807 nm) was performed with a maximum achieved output power of 31.5 mW and 141 mW, respectively. The pulse compression was implemented by a pair of gratings, leading to pulse durations of 523 fs at 1708 nm and 478 fs at 1807 nm. The demonstrated tunable dissipative soliton laser and power scalability in the short-wavelength-band of the Tm-doped fiber operational region can facilitate applications ranging from advanced bioimaging to material processing.

Funding. European Commission (871277); Academy of Finland (320165); Engineering and Physical Sciences Research Council (EP/N00762X/1).

Disclosures. The authors declare no conflicts of interest.

Data availability. Data underlying the results presented in this paper are not publicly available at this time but may be obtained from the authors upon reasonable request.

REFERENCES

1. S. D. Jackson, Nat. Photonics **6**, 423 (2012).
2. P. J. Roberts, F. Couny, H. Sabert, B. J. Mangan, D. P. Williams, L. Farr, M. W. Mason, A. Tomlinson, T. A. Birks, J. C. Knight, and P. S. J. Russell, Opt. Express **13**, 236 (2005).
3. I. Mingareev, F. Weirauch, A. Olowinsky, L. Shah, P. Kadwani, and M. Richardson, Opt. Laser Technol. **44**, 2095 (2012).
4. R. R. Anderson, W. Farinelli, H. Laubach, D. Manstein, A. N. Yaroslavsky, J. Gubeli, K. Jordan, G. R. Neil, M. Shinn, W. Chandler, G. P. Williams, S. V. Benson, D. R. Douglas, and H. F. Dylla, Lasers Surg. Med. **38**, 913 (2006).
5. S. Kurilchik, M. Gacci, R. Cicchi, F. S. Pavone, S. Morselli, S. Serni, M. H. Chou, M. Närhi, E. Rafailov, N. Stewart, C. Lennon, and R. Gumenyuk, JPhys Photonics **2**, 021001 (2020).
6. Y. Tang, A. Chong, and F. W. Wise, Opt. Lett. **40**, 2361 (2015).
7. R. Gumenyuk, I. Vartiainen, H. Tuovinen, and O. G. Okhotnikov, Opt. Lett. **36**, 609 (2011).
8. L. E. Nelson, E. P. Ippen, and H. A. Haus, Appl. Phys. Lett. **67**, 19 (1995).
9. J. Shang, S. Zhao, Y. Liu, K. Yang, C. Wang, Y. Zhao, Y. Song, P. Hu, J. Mao, T. Li, and T. Feng, Opt. Laser Technol. **153**, 108206 (2022).
10. S. Agger, P. Varming, and J. H. Povlsen, Fiber Lasers: Technology, Systems, and Applications. **5335**, SPIE (2004).
11. M. Yamada, K. Senda, T. Tanaka, Y. Maeda, S. Aozasa, H. Ono, K. Ota, O. Koyama, and J. Ono, Electron. Lett. **49**, 1287 (2013).
12. S. D. Emami, A. Khodaei, S. Gandan, R. Penny, K. S. Lim, H. A. Abdul-Rashid, and H. Ahmad, Opt. Express **23**, 19681 (2015).
13. Z. Li, Y. Jung, J. M. O. Daniel, N. Simakov, M. Tokurakawa, P. C. Shardlow, D. Jain, J. K. Sahu, A. M. Heidt, W. A. Clarkson, S. U. Alam, and D. J. Richardson, Opt. Lett. **41**, 2197 (2016).
14. S. Chen, Y. Chen, K. Liu, R. Sidharthan, H. Li, C. J. Chang, Q. J. Wang, D. Tang, and S. Yoo, Opt. Express **28**, 17570 (2020).
15. S. D. Emami, M. M. Dashtabi, H. J. Lee, A. S. Arabanian, and H. A. A. Rashid, Sci. Rep. **7**, 12747 (2017).
16. T. Noronen, O. Okhotnikov, and R. Gumenyuk, Opt. Express **24**, 14703 (2016).
17. R. Dai, Y. Meng, Y. Li, J. Qin, S. Zhu, and F. Wang, Opt. Express **27**, 3518 (2019).
18. J.-X. Chen, Z.-Y. Zhan, C. Li, M. Liu, A.-P. Luo, P. Zhou, W.-C. Xu, and Z.-C. Luo, Opt. Lett. **46**, 5922 (2021).
19. J.-X. Chen, X.-Y. Li, T.-J. Li, Z.-Y. Zhan, M. Liu, C. Li, A.-P. Luo, P. Zhou, K. K.-Y. Wong, W.-C. Xu, and Z.-C. Luo, Photonics Res. **9**, 873 (2021).
20. L. Bei, Prog. Quantum Electron. **28**, 67 (2004).
21. X. Liu, M. Närhi, D. Korobko, and R. Gumenyuk, Opt. Express **29**, 34977 (2021).
22. Z.-W. Lin, J.-X. Chen, T.-J. Li, Z.-Y. Zhan, M. Liu, C. Li, A.-P. Luo, P. Zhou, W.-C. Xu, and Z.-C. Luo, Opt. Express **30**, 32347 (2022).
23. W. S. Man, H. Y. Tam, M. S. Demokan, P. K. A. Wai, and D. Y. Tang, J. Opt. Soc. Am. B **17**, 28 (2000).
24. Chin Yu Chong, "Femtosecond fiber lasers and amplifiers based on the pulse propagation at normal dispersion," (2008).
25. P. Elahi, S. Yılmaz, Ö Akçaalan, H. Kalaycıoğlu, B. Öktem, CÇ Şeşenel, FÖ Ilday, and K. Eken, Opt. Lett. **37**, 3042 (2012).
26. R. T. Schermer and J. H. Cole, IEEE J. Quantum Electron. **43**, 899 (2007).
27. L. Faustini and G. Martini, J. Lightwave Technol. **15**, 671 (1997).
28. M. Närhi, A. Fedotov, K. Aksenova, J. Fiebrandt, T. Schönau, M. Gerecke, and R. Gumenyuk, Opt. Express **29**, 15699 (2021).